Contemporary Mathematics
Volume **526**, 2010

Potential based, constraint preserving, genuinely multi-dimensional schemes for systems of conservation laws

Siddhartha Mishra and Eitan Tadmor

Abstract. We survey the new framework developed in [**33, 34, 35**], for designing genuinely multi-dimensional (GMD) finite volume schemes for systems of conservation laws in two space dimensions. This approach is based on reformulating edge centered numerical fluxes in terms of *v*ertex centered potentials. *Any* consistent numerical flux can be used in defining the potentials. Suitable choices of the numerical potentials yield finite-volume schemes which preserve discrete form of constraints such as vorticity and divergence. The schemes are very simple to code, flexible and have low computational costs. Numerical examples for the Euler equations of gas dynamics and the ideal MHD equations are presented to illustrate the computational efficiency of the schemes.

1. Introduction

Many interesting phenomena in physics, engineering and biology are modeled by hyperbolic systems of conservation laws. In two space dimensions, these equations take the form

$$\mathbf{U}_t + \mathbf{f}(\mathbf{U})_x + \mathbf{g}(\mathbf{U})_y = 0, \quad (x, y, t) \in \mathbb{R} \times \mathbb{R} \times \mathbb{R}_+, \tag{1.1}$$

where $\mathbf{U}$ is the vector of unknowns and $\mathbf{f}, \mathbf{g}$ are the flux vectors in the x- and y-directions respectively.

A frequently cited example of the system (1.1) are the Euler equations of gas dynamics,

$$\begin{aligned} \rho_t + (\rho u_1)_x + (\rho u_2)_y &= 0, \\ (\rho u_1)_t + (\rho u_1^2 + p)_x + (\rho u_1 u_2)_y &= 0, \\ (\rho u_2)_t + (\rho u_1 u_2)_x + (\rho u_2^2 + p)_y &= 0, \\ E_t + ((E + p)u_1)_x + ((E + p)u_2)_y &= 0, \end{aligned} \tag{1.2a}$$

1991 *Mathematics Subject Classification.* 65M06,35L65.

Key words and phrases. multidimensional evolution equations, nonlinear conservation laws, constraint transport, central difference schemes, potential-based fluxes.

Acknowledgment. The work on this paper began when S.M. visited the Center of Scientific Computation and Mathematical Modeling (CSCAMM) and he thanks CSCAMM and all its members for the excellent hospitality and facilities. E. T. Research was supported in part by NSF grant 07-07949 and ONR grant N00014-091-0385. He thanks the Centre for Advanced Study at the Norwegian Academy of Science and Letters, for hosting him as part of its international research program on Nonlinear PDEs during the academic year 2008-09.

with ρ being the density of the gas, u_1, u_2 are the velocity components in the x- and y-direction respectively and p and E are the pressure and the energy. The equations are augmented by an ideal gas equation of state, which is expressed in terms of the gas constant γ:

$$E = \frac{p}{\gamma - 1} + \frac{1}{2}(\rho u_1^2 + \rho u_2^2). \tag{1.2b}$$

Other interesting examples for hyperbolic systems are the shallow water equations of oceanography and the equations of non-linear elasticity.

It is well known that solutions of (1.1) (even in one space dimension) develop discontinuities in the form of *shock waves*, even for smooth initial data. Hence, the solutions sought for (1.1) are defined in a weak sense. Weak solutions are not necessarily unique and (1.1) has to be supplemented by additional admissibility criteria, the so-called *entropy conditions* [**12**]. The existence and uniqueness theory for multi-dimensional scalar conservation laws and for some special cases of one- and multi-dimensional systems is well developed. A corresponding theory for multi-dimensional systems is still "work in progress".

1.1. Finite-volume schemes. Explicit formulas for the solution of (1.1) are not available, except in the simplest cases. Consequently, numerical methods are heavily used for approximating (1.1). The most popular numerical methods in this context are the finite volume schemes, see e.g., [**28, 45**] and references therein for a detailed description. In a finite volume approximation, the computational domain is discretized into cells or control volumes and an integral form of the conservation law (1.1) is approximated on each control volume. This method relies on constructing suitable numerical fluxes in the normal direction, across each cell interface. For simplicity, a uniform Cartesian discretization of the domain is considered, with mesh sizes Δx and Δy in the x- and y- directions respectively. It consists of the discrete cells, $\mathcal{C}_{i,j} := [x_{i-\frac{1}{2}}, x_{i+\frac{1}{2}}) \times [y_{j-\frac{1}{2}}, y_{j+\frac{1}{2}})$, centered at the mesh points $(x_i, y_j) = (i\Delta x, j\Delta y)$, $(i,j) \in \mathbb{Z}^2$. The cell average of $\mathbf{U}$ over $\mathcal{C}_{i,j}$ (at time t), denoted $\mathbf{U}_{i,j}(t)$, is updated with the semi-discrete scheme [**28, 45**]:

$$\frac{d}{dt}\mathbf{U_{i,j}} = -\frac{1}{\Delta x}(\mathbf{F}_{i+\frac{1}{2},j} - \mathbf{F}_{i-\frac{1}{2},j}) - \frac{1}{\Delta y}(\mathbf{G}_{i,j+\frac{1}{2}} - \mathbf{G}_{i,j-\frac{1}{2}}). \tag{1.3}$$

The time dependence of all the quantities in the above expression is suppressed for notational convenience. Classical schemes employ two-point numerical fluxes,

$$\mathbf{F}_{i+\frac{1}{2},j} = \mathbf{F}(\mathbf{U}_{i,j}, \mathbf{U}_{i+1,j}), \quad \mathbf{G}_{i,j+\frac{1}{2}} = \mathbf{G}(\mathbf{U}_{i,j}, \mathbf{U}_{i,j+1}).$$

A canonical example is provided by the first-order Rusanov numerical flux:

(1.4)

$$\mathbf{F}_{i+\frac{1}{2},j} = \frac{1}{2}\big(\mathbf{f}(\mathbf{U}_{i,j}) + \mathbf{f}(\mathbf{U}_{i+1,j})\big) - \max\{|(\alpha)_{i,j}|, |(\alpha)_{i+1,j}|\}\big(\mathbf{U}_{i+1,j} - \mathbf{U}_{i,j}\big),$$

$$\mathbf{G}_{i,j+\frac{1}{2}} = \frac{1}{2}\big(\mathbf{g}(\mathbf{U}_{i,j}) + \mathbf{g}(\mathbf{U}_{i,j+1})\big) - \max\{|(\beta)_{i,j}|, |(\beta)_{i,j+1}|\}\big(\mathbf{U}_{i,j+1} - \mathbf{U}_{i,j}\big).$$

Here, $\alpha_{i,j}$ and $\beta_{i,j}$ are the maximal eigenvalues of the Jacobians $\mathbf{A} = \partial_{\mathbf{U}}\mathbf{f}$ and $\mathbf{B} = \partial_{\mathbf{U}}\mathbf{g}$ respectively, for a given state $\mathbf{U}_{i,j}$:

$$\alpha_{i,j} := \mathrm{argmax}_\lambda\{|\lambda| : \lambda = \lambda\big(\mathbf{A}(\mathbf{U_{i,j}})\big)\}, \quad \beta_{i,j} = \mathrm{argmax}_\lambda\{|\lambda| : \lambda = \lambda\big(\mathbf{B}(\mathbf{U_{i,j}})\big)\}.$$

Note that the only characteristic information in the Rusanov flux is a local estimate on the wave speeds. This flux is almost Jacobian free, very simple to implement

and has a very low computational cost. But its resolution is limited by the first-order accuracy. But the first-order schemes (1.3),(1.4) can be extended to higher order accuracy by employing numerical fluxes based on wider, $2p$-point stencils, $I_{i+\frac{1}{2}} := \{i' \,|\, |i'-i-1/2| < p\}$ and $J_{j+\frac{1}{2}} := \{j' \,|\, |j'-j-1/2| < p\}$ along the x- and y-axis, respectively,

$$\mathbf{F}_{i+\frac{1}{2},j} = \mathbf{F}\Big(\{\mathbf{U}_{i',j}\}_{i'\in I_{i+\frac{1}{2}}}\Big), \quad \mathbf{G}_{i,j+\frac{1}{2}} = \mathbf{G}\Big(\{\mathbf{U}_{i,j'}\}_{j'\in J_{j+\frac{1}{2}}}\Big). \tag{1.5}$$

The building blocks for such extensions are still the 2-point numerical fluxes, $\mathbf{F}(\cdot,\cdot)$ and $\mathbf{G}(\cdot,\cdot)$. As a prototype example, we recall the class of second-order schemes based on piecewise bilinear MUSCL reconstruction [**27**]

$$\mathbf{p}_{i,j}(x,y) := \mathbf{U}_{i,j} + \frac{\mathbf{U}'_{i,j}}{\Delta x}(x-x_i) + \frac{\mathbf{U}'_{i,j}}{\Delta y}(y-y_j); \tag{1.6a}$$

Here, $\mathbf{U}'$ and $\mathbf{U}'$ denote the *numerical derivatives*

$$\begin{aligned} \mathbf{U}'_{i,j} &= \text{minmod}(\mathbf{U}_{i+1,j}-\mathbf{U}_{i,j}, \frac{1}{2}(\mathbf{U}_{i+1,j}-\mathbf{U}_{i-1,j}), \mathbf{U}_{i,j}-\mathbf{U}_{i-1,j}), \\ \mathbf{U}'_{i,j} &= \text{minmod}(\mathbf{U}_{i,j+1}-\mathbf{U}_{i,j}, \frac{1}{2}(\mathbf{U}_{i,j+1}-\mathbf{U}_{i,j-1}), \mathbf{U}_{i,j}-\mathbf{U}_{i,j-1}), \end{aligned} \tag{1.6b}$$

which utilize the minmod limiter

$$\text{minmod}(a,b,c) = \begin{cases} \text{sgn(a)}\,\min\{|a|,|b|,|c|\}, & \text{if} \quad \text{sgn(a)} = \text{sgn(b)} = \text{sgn(c)}, \\ 0, & \text{otherwise.} \end{cases} \tag{1.6c}$$

In this manner, one can reconstruct in each cell $\mathcal{C}_{i,j}$, the point values

$$\begin{cases} \mathbf{U}^E_{i,j} := \mathbf{p}_{i,j}(x_{i+\frac{1}{2}}, y_j), & \mathbf{U}^W_{i,j} := \mathbf{p}_{i,j}(x_{i-\frac{1}{2}}, y_j), \\ \mathbf{U}^N_{i,j} := \mathbf{p}_{i,j}(x_i, y_{j+\frac{1}{2}}), & \mathbf{U}^S_{i,j} := \mathbf{p}_{i,j}(x_i, y_{j-\frac{1}{2}}), \end{cases} \tag{1.7a}$$

from the given neighboring cell averages $\mathbf{U}_{i,j}, \mathbf{U}_{i\pm1,j}$ and $\mathbf{U}_{i,j}, \mathbf{U}_{i,j\pm1}$. The resulting second-order fluxes are then given by

$$\mathbf{F}_{i+\frac{1}{2},j} = \mathbf{F}(\mathbf{U}^E_{i,j}, \mathbf{U}^W_{i+1,j}), \quad \mathbf{G}_{i,j+\frac{1}{2}} = \mathbf{G}(\mathbf{U}^N_{i,j}, \mathbf{U}^S_{i,j+1}). \tag{1.7b}$$

The use of minmod limiter ensures the non-oscillatory behavior of the second-order schemes (1.3),(1.6). Observe that the second-order MUSCL fluxes (1.7b) are based on 4-point stencils

$$\mathbf{F}_{i+\frac{1}{2},j} = \mathbf{F}(\mathbf{U}_{i-1,j}, \mathbf{U}_{i,j}, \mathbf{U}_{i+1,j}, \mathbf{U}_{i+2,j}), \quad \mathbf{G}_{i,j+\frac{1}{2}} = \mathbf{F}(\mathbf{U}_{i,j-1}, \mathbf{U}_{i,j}, \mathbf{U}_{i,j+1}, \mathbf{U}_{i,j+2})$$

Similar reconstructions together with upwind or central averaging yield a large class of high-resolution finite-volume semi-discrete schemes, e.g., [**23**],[**44**],[**25**], which could then be integrated in time using standard stable high order Runge-Kutta methods [**22**].

1.2. Genuinely multi-dimensional (GMD) schemes. Despite their considerable success in many applications, finite volume schemes (1.3) are known to be deficient [**28**] in resolving genuinely multi-dimensional waves in the solution of (1.1). A possible explanation lies in the structure of the scheme (1.3). The numerical fluxes $\mathbf{F}_{i+\frac{1}{2},j}, \mathbf{G}_{i,j+\frac{1}{2}}$ are defined in each normal direction and lack explicit transverse information. Considerable effort has been devoted to devising *genuinely multi-dimensional* (GMD) finite volume schemes for approximating (1.1). We provide a very brief summary of some of the available methods:

(i) *Dimensional splitting.* This procedure is based on sequentially updating the cell average with flux $\mathbf{F}_{i+\frac{1}{2},j}$ (in the x-direction) and then updating with the numerical flux $\mathbf{G}_{i,j+\frac{1}{2}}$ (in the y- direction). Second order accuracy results from Strang splitting [**28**]. Despite the splitting, the resulting method may still fail to resolve genuinely multi-dimensional waves (examples are provided in [**29**]).

(ii) *Multi-dimensional wave propagation.* This method is based on the Corner Transport Upwind (CTU) method [**11**] for linear equations. Contributions from waves in the transverse direction are explicitly calculated. It was extended to non-linear systems in [**29**] by solving transverse Riemann problems. The method is implemented in the *CLAWPACK* software package [**28**]. A related scheme was proposed in [**8**].

(iii) *Method of Transport.* In [**17, 18, 38**], the non-linear conservation law (1.1) is reformulated locally as a system of transport equations. Explicit solutions of the transport equations define a genuinely multi-dimensional scheme. Complicated formulas for specific wave models may be a major disadvantage of this method.

(iv) *Finite volume Evolution Galerkin (FVEG) methods.* In [**30, 31**] (and other references therein), the conservation law (1.1) is linearized locally and the linearized system is solved in terms of bi-characteristics. The resulting evolution operator defines genuinely multi-dimensional finite volume fluxes by a Galerkin type approximation. The task of deriving explicit solutions in terms of bi-characteristics for specific models may be quite complicated.

(v) *Residual distribution/Fluctuation-splitting schemes.* Genuinely multi-dimensional methods for unstructured meshes were proposed in [**14, 2, 37**]. They involve computing a cell residual at each time step and distributing it to the cell nodes by using some suitable upwinding procedure, based on local flow directions.

The absence of an optimal strategy for genuinely multi-dimensional schemes leaves room for designing stable GMD schemes that are easy to formulate and code, have a low computational cost and preserve other desirable properties shared by the multi-dimensional structure of the system (1.1). Their numerical fluxes take a general form

$$\mathbf{F}_{i+\frac{1}{2},j} = \mathbf{F}(\{\mathbf{U}_{(i',j')\in S_{i+\frac{1}{2},j}}\}), \quad \mathbf{G}_{i,j+\frac{1}{2}} = \mathbf{G}(\{\mathbf{U}_{(i',j')\in S_{i,j+\frac{1}{2}}}\}). \tag{1.8a}$$

Here, $S_{i+\frac{1}{2},j}$ and $S_{i,j+\frac{1}{2}}$ are *two-dimensional* stencils which, in contrast to (1.5), allow us to incorporate information from both the normal and transverse directions,

$$S_{i+\frac{1}{2},j} := \big\{(i',j') \,\big|\, |i'-i-1/2|+|j'-j| < q\big\},\ S_{i,j+\frac{1}{2}} := \big\{(i',j') \,\big|\, |i'-i|+|j'-j-1/2| < q\big\} \tag{1.8b}$$

We present such a family of GMD schemes in section 2.

1.3. Conservation laws with constraints. Many interesting multi-dimensional systems of conservation laws also involve *intrinsic* constraints. A representative example for such a system are the magnetohydrodynamic (MHD) equations of plasma

physics:

$$
\begin{aligned}
\rho_t + (\rho u_1)_x + (\rho u_2)_y &= 0,\\
(\rho u_1)_t + (\rho (u_1)^2 + \widetilde{p} - \frac{1}{2}(B_1)^2)_x + (\rho u_1 u_2 - B_1 B_2)_y &= 0,\\
(\rho u_2)_t + (\rho u_1 u_2 - B_1 B_2)_x + (\rho (u_2)^2 + \widetilde{p} - \frac{1}{2}(B_2)^2)_y &= 0,\\
(\rho u_3)_t + (\rho u_1 u_3 - B_1 B_3)_x + (\rho u_2 u_3 - B_2 B_3)_y &= 0,\\
(B_1)_t + (u_2 B_1 - u_1 B_2)_y &= 0,\\
(B_2)_t + (u_1 B_2 - u_2 B_1)_x &= 0,\\
(B_3)_t + (u_1 B_3 - u_3 B_1)_x + (u_2 B_3 - u_3 B_2)_y &= 0,\\
E_t + ((E + \widetilde{p}) u_1 - (\mathbf{u}\cdot\mathbf{B}) B_1)_x + ((E + \widetilde{p}) u_2 - (\mathbf{u}\cdot\mathbf{B}) B_2)_y &= 0,
\end{aligned}
\tag{1.9}
$$

where the density of the plasma is denoted by ρ, $\mathbf{u} = (u_1, u_2, u_3)^\top$ and $\mathbf{B} = (B_1, B_2, B_3)^\top$ are the velocity and magnetic fields, respectively. E is the total energy and $\widetilde{p} := p + \frac{1}{2}|\mathbf{B}|^2$ is the total pressure, with p being the thermal pressure. The unknowns are related by an ideal gas equation of state similar to (1.2b). The ideal MHD equations (1.9) form a (non-strictly) hyperbolic system of conservation laws, which combine the conservation laws for mass, momentum and energy with the magnetic induction equations (a special form of the Maxwell's equations):

$$
\mathbf{B}_t + \operatorname{curl}(\mathbf{B}\times\mathbf{u}) = 0, \quad (x, y, t) \in \mathbb{R}\times\mathbb{R}\times\mathbb{R}_+,
\tag{1.10}
$$

which implies the divergence constraint,

$$
\operatorname{div}(\mathbf{B})_t \equiv 0.
\tag{1.11a}
$$

In the particular two-dimensional setup of (1.9), the divergent constraint is reduced to the two-component statement

$$
\operatorname{div}\big((B_1, B_2)^\top\big)_t \equiv 0.
\tag{1.11b}
$$

Since magnetic monopoles have not been observed in nature, the initial magnetic field is assumed to be divergence free. The divergence constraint (1.11) implies that the divergence of the magnetic field remains zero. Hence, the ideal MHD equations are an example for multi-dimensional systems of conservation laws with an intrinsic constraint.

Other interesting examples for systems with constraints are the system wave equation [**36**] (with vorticity as the constraint) and the Einstein equations of general relativity.

A major issue for the numerical approximation of multi-dimensional ideal MHD equations (1.9) is the divergence constraint (1.11). The failure of standard finite volume schemes to preserve discrete versions of that constraint may lead to numerical instabilities [**48, 19**]. Different approaches have been suggested to handle the divergence constraint in MHD codes. We describe some of them briefly.

(i) *Projection method.* This method [**10, 7, 6**] is based on the Hodge decomposition of the magnetic field $\mathbf{B}$. The update $\mathbf{B}^n$, at each time step, may not be divergence free and is corrected by the decomposition: $\mathbf{B}^n = \nabla\Psi + \operatorname{curl}\Phi$. Applying the divergence operator to the decomposition leads to the elliptic equation:

$$
-\Delta\Psi = \operatorname{div}(\mathbf{B}^n).
$$

The corrected field $\mathbf{B}^* = \mathbf{B}^n - \nabla\Psi$ is divergence free. This method can be very expensive computationally as an elliptic equation has to be solved at every time step.

(ii) *Source terms.* Adding a source term, proportional to the divergence, in (1.10) results in

$$\mathbf{B}_t + \mathrm{curl}(\mathbf{B} \times \mathbf{u}) = -\mathbf{u}(\mathrm{div}(\mathbf{B})).$$

Applying the divergence operator to both sides:

$$\mathrm{div}(\mathbf{B})_t + \mathrm{div}(\mathbf{u}(\mathrm{div}\mathbf{B})) = 0.$$

Hence any potential divergence errors are transported away from the computational domain by the flow. This procedure for "cleaning the divergence" was introduced in [**39, 40**] and it needs to be discretized in a very careful manner in order to avoid two main difficulties: to keep numerical stability [**19, 20**] and to avoid a wrong shock speed due to the non-conservative form of the source term [**48**]. A variant of this approach is the Generalized Lagrange multiplier method [**15**].

(iii) *Design of special divergence operators/staggering.* This popular method consists of staggering the discretizations of the velocity and magnetic fields in (1.10). A wide variety of strategies for staggering the meshes has been proposed, [**16, 5, 13, 43, 48, 4**] and references therein. The presence of different sets of meshes leads to problems when parallelizing this method and using adaptive mesh refinement. Unstaggered variants of this approach have also been proposed in [**47, 46, 1**].

The above discussion suggests there is ample scope for a simple, computationally cheap finite volume scheme for the MHD equations that resolves genuinely multi-dimensional waves and preserves a discrete version of the divergence constraint. Our aim in this paper is to summarize the results of recent papers [**33, 34, 35**] and present a new framework for approximating the two-dimensional conservation law (1.1) in a genuinely multi-dimensional manner. The GMD scheme is designed by rewriting the standard finite volume scheme (1.3) in terms of vertex centered *numerical potentials*. Standard edge centered numerical fluxes serve as building blocks of the GMD scheme as the numerical potential is defined in terms of them. The choice of potentials is very general and a specific choice of potential results in an *entropy stable* GMD scheme [**34**, §3]. In particular, in section 4 we discuss potential-based GMD schemes that preserve a discrete version of the divergence in the MHD equations. Numerical experiments illustrating the robustness of the schemes in approximating the Euler equations (1.2a) and the ideal MHD equations (1.9) are presented.

2. Genuinely multi-dimensional (GMD) schemes

Following the presentation of [**34**], we introduce the *numerical potentials* $\phi_{i+\frac{1}{2},j+\frac{1}{2}}$ and $\psi_{i+\frac{1}{2},j+\frac{1}{2}}$ at each vertex $(x_{i+\frac{1}{2}}, y_{j+\frac{1}{2}})$, with the sole requirement that these potentials are consistent with the differential fluxes, i.e,

$$\phi_{i+\frac{1}{2},j+\frac{1}{2}}(\mathbf{U},\cdots,\mathbf{U}) = \mathbf{f}(\mathbf{U}), \quad \psi_{i+\frac{1}{2},j+\frac{1}{2}}(\mathbf{U},\cdots,\mathbf{U}) = \mathbf{g}(\mathbf{U}).$$

We need the following notation for standard averaging and (undivided) difference operators,

$$\begin{aligned} \mu_x a_{I,J} &:= \frac{a_{I+\frac{1}{2},J} + a_{I-\frac{1}{2},J}}{2}, \quad \mu_y a_{I,J} := \frac{a_{I,J+\frac{1}{2}} + a_{I,J-\frac{1}{2}}}{2}, \\ \delta_x a_{I,J} &:= a_{I+\frac{1}{2},J} - a_{I-\frac{1}{2},J}, \quad \delta_y a_{I,J} := a_{I,J+\frac{1}{2}} - a_{I,J-\frac{1}{2}}. \end{aligned} \tag{2.1}$$

A word about our notations: we note that the above discrete operators could be used with indexes I, J which are placed at the center or at the edge of the computational cells, e.g., $I = i$ or $I = i + \frac{1}{2}$. In either case, we tag the resulting discrete operators according to the center of their stencil; thus, for example, $\mu_x w_{i+\frac{1}{2}}$ employs grid values placed on the integer-indexed edges, w_i and w_{i+1}, whereas $\delta_y w_j$ employs the half-integer indexed centers, $w_{j\pm\frac{1}{2}}$.

We now set the numerical fluxes:

$$\begin{aligned} \mathbf{F}_{i+\frac{1}{2},j} &= \mu_y \phi_{i+\frac{1}{2},j}, \\ \mathbf{G}_{i,j+\frac{1}{2}} &= \mu_x \phi_{i,j+\frac{1}{2}}. \end{aligned} \tag{2.2}$$

The resulting finite volume scheme written in terms of the numerical potentials reads

$$\begin{aligned} \frac{d}{dt}\mathbf{U}_{i,j} &= -\frac{1}{\Delta x}\delta_x \mu_y \phi_{i,j} - \frac{1}{\Delta y}\delta_y \mu_x \psi_{i,j}, \\ &= -\frac{1}{\Delta x}\Big(\frac{1}{2}(\phi_{i+\frac{1}{2},j+\frac{1}{2}} + \phi_{i+\frac{1}{2},j-\frac{1}{2}}) - \frac{1}{2}(\phi_{i-\frac{1}{2},j+\frac{1}{2}} + \phi_{i-\frac{1}{2},j-\frac{1}{2}})\Big) \\ &\quad - \frac{1}{\Delta y}\Big(\frac{1}{2}(\psi_{i+\frac{1}{2},j+\frac{1}{2}} + \psi_{i-\frac{1}{2},j+\frac{1}{2}}) - \frac{1}{2}(\psi_{i+\frac{1}{2},j-\frac{1}{2}} + \psi_{i-\frac{1}{2},j-\frac{1}{2}})\Big). \end{aligned} \tag{2.3}$$

The potential based scheme (2.3) is clearly conservative as well as consistent as the potentials ϕ, ψ are consistent. The genuinely multi-dimensional nature of the scheme is evident from (2.3): the potentials are differenced in the normal direction but averaged in the transverse direction. We claim that the family of potential-based schemes (2.3) is *rich*: any standard finite volume flux can be used as a building block for constructing the numerical potentials in (2.2), and the resulting potential-based scheme inherits the accuracy of the underlying numerical flux. There are several ways to pursue the construction of numerical potentials and we outlined four of them below.

2.1. Symmetric potentials. In this approach, the potentials are defined by averaging the finite volume fluxes neighboring a vertex:

$$\begin{aligned} \phi_{i+\frac{1}{2},j+\frac{1}{2}} &= \mu_y \mathbf{F}_{i+\frac{1}{2},j+\frac{1}{2}}, \\ \psi_{i+\frac{1}{2},j+\frac{1}{2}} &= \mu_x \mathbf{G}_{i+\frac{1}{2},j+\frac{1}{2}}, \end{aligned} \tag{2.4}$$

where $\mathbf{F}_{i+\frac{1}{2},j}$ and $\mathbf{G}_{i,j+\frac{1}{2}}$ are *any* numerical fluxes consistent with $\mathbf{f}$ and $\mathbf{g}$ respectively. An explicit computation of (2.3) with potentials (2.4) leads to the revealing form,

$$\begin{aligned} \frac{d}{dt}\mathbf{U}_{i,j} = &-\frac{1}{2\Delta x}(\mu_y \mathbf{F}_{i+\frac{1}{2},j+\frac{1}{2}} + \mu_y \mathbf{F}_{i+\frac{1}{2},j-\frac{1}{2}} - \mu_y \mathbf{F}_{i-\frac{1}{2},j+\frac{1}{2}} - \mu_y \mathbf{F}_{i-\frac{1}{2},j-\frac{1}{2}}) \\ &- \frac{1}{2\Delta y}(\mu_x \mathbf{G}_{i+\frac{1}{2},j+\frac{1}{2}} + \mu_x \mathbf{G}_{i-\frac{1}{2},j+\frac{1}{2}} - \mu_x \mathbf{G}_{i+\frac{1}{2},j-\frac{1}{2}} - \mu_x \mathbf{G}_{i-\frac{1}{2},j-\frac{1}{2}}). \end{aligned} \tag{2.5}$$

Comparing the potential based scheme (2.5) with the standard finite volume scheme (1.3), we observe that the potential based scheme modifies (1.3) by averaging the fluxes in the transverse direction. Hence, it incorporates *explicit* transverse information in each direction. When employing two-point fluxes, the local stencil for the GMD scheme (2.5) consists of nine points instead of the standard five point stencil for the finite volume scheme (1.3). One can use wider stencils to achieve higher-order of accuracy; for example, the symmetric potential-based scheme based on second-order four-point MUSCL flux (1.6) yields a second-order GMD scheme based on a stencil of twenty-three points.

2.2. Weighted symmetric potentials. Weighted averages of the neighboring fluxes can be considered in place of the simple averaging used in (2.4). For prescribed $\theta_{i+\frac{1}{2},j+\frac{1}{2}}, \kappa_{i+\frac{1}{2},j+\frac{1}{2}} \in (0,1)$, the weighted potential is defined as

$$\begin{aligned} \phi_{i+\frac{1}{2},j+\frac{1}{2}} &= \theta_{i+\frac{1}{2},j+\frac{1}{2}}\mathbf{F}_{i+\frac{1}{2},j+1} + (1-\theta_{i+\frac{1}{2},j+\frac{1}{2}})\mathbf{F}_{i+\frac{1}{2},j}, \\ \psi_{i+\frac{1}{2},j+\frac{1}{2}} &= \kappa_{i+\frac{1}{2},j+\frac{1}{2}}\mathbf{G}_{i+1,j+\frac{1}{2}} + (1-\kappa_{i+\frac{1}{2},j+\frac{1}{2}})\mathbf{G}_{i,j+1/2}. \end{aligned} \tag{2.6}$$

The weights can be chosen based on the local characteristic speeds,

$$\begin{aligned} \theta_{i+\frac{1}{2},j+\frac{1}{2}} &= \frac{\max\{-(\beta_1)_{i+\frac{1}{2},j+\frac{1}{2}},0\}}{\max\{-(\beta_1)_{i+\frac{1}{2},j+\frac{1}{2}},0\}+\max\{(\beta_N)_{i+\frac{1}{2},j+\frac{1}{2}},0\}}, \\ \kappa_{i+\frac{1}{2},j+\frac{1}{2}} &= \frac{\max\{-(\alpha_1)_{i+\frac{1}{2},j+\frac{1}{2}},0\}}{\max\{-(\alpha_1)_{i+\frac{1}{2},j+\frac{1}{2}},0\}+\max\{(\alpha_N)_{i+\frac{1}{2},j+\frac{1}{2}},0\}}. \end{aligned} \tag{2.7}$$

Here, α_l and , $\beta_l, l = 1, 2, \cdots, N$ are the real eigenvalues of $A = \partial_{\mathbf{U}}\mathbf{f}(\mu_y\mu_x\mathbf{U}_{i+\frac{1}{2},j+\frac{1}{2}})$ and $B = \partial_{\mathbf{U}}\mathbf{g}(\mu_x\mu_y\mathbf{U}_{i+\frac{1}{2},j+\frac{1}{2}})$, sorted in an increasing order. This choice of weights means that the potential (2.6) is "upwinded" i.e, takes local flow directions into account.

2.3. Staggered potentials. We define the numerical potential as

$$\phi_{i+\frac{1}{2},j+\frac{1}{2}} = \mathbf{F}(\mu_y\mathbf{U}_{i,j+\frac{1}{2}}, \mu_y\mathbf{U}_{i+1,j+\frac{1}{2}}), \quad \psi_{i+\frac{1}{2},j+\frac{1}{2}} = \mathbf{G}(\mu_x\mathbf{U}_{i+\frac{1}{2},j}, \mu_x\mathbf{U}_{i+\frac{1}{2},j+1}) \tag{2.8}$$

for any consistent numerical fluxes $\mathbf{F}, \mathbf{G}$.

2.4. Diagonal potentials. We define the diagonal potentials [**33**] ,

$$\begin{aligned} \phi_{i+\frac{1}{2},j+\frac{1}{2}} &= \frac{1}{2}\big(\mathbf{F}^+_{i+\frac{1}{2},j+\frac{1}{2}} + \mathbf{F}^-_{i+\frac{1}{2},j+\frac{1}{2}}\big), \\ \psi_{i+\frac{1}{2},j+\frac{1}{2}} &= \frac{1}{2}(\mathbf{G}^+_{i+\frac{1}{2},j+\frac{1}{2}} + \mathbf{G}^-_{i+\frac{1}{2},j+\frac{1}{2}}). \end{aligned} \tag{2.9a}$$

Here, $\mathbf{F}^\pm, \mathbf{G}^\pm$ are the *diagonal* fluxes

$$\begin{aligned} \mathbf{F}^+_{i+\frac{1}{2},j+\frac{1}{2}} &:= \mathbf{F}(\mathbf{U}_{i,j}, \mathbf{U}_{i+1,j+1}), \quad \mathbf{F}^-_{i+\frac{1}{2},j-\frac{1}{2}} = \mathbf{F}(\mathbf{U}_{i,j}, \mathbf{U}_{i+1,j-1}) \\ \mathbf{G}^+_{i+\frac{1}{2},j+\frac{1}{2}} &:= \mathbf{G}(\mathbf{U}_{i,j}, \mathbf{U}_{i+1,j+1}), \quad \mathbf{G}^-_{i-\frac{1}{2},j+\frac{1}{2}} := \mathbf{G}(\mathbf{U}_{i,j}, \mathbf{U}_{i-1,j+1}). \end{aligned} \tag{2.9b}$$

which amount to rotating the x- and y-axis by angles of $\frac{\pi}{4}$ and $-\frac{\pi}{4}$ and $\mathbf{F}(\cdot,\cdot)$ and $\mathbf{G}(\cdot,\cdot)$ are any two-point numerical fluxes consistent with $\mathbf{f}$ and $\mathbf{g}$.

We conclude our list for recipes of GMD schemes with an example which is *not* rendered by a numerical potential, but nevertheless, highlights the use of a GMD stencil.

Let $\mathbf{F}(\cdot,\cdot)$ and $\mathbf{G}(\cdot,\cdot)$ are any two-point consistent numerical fluxes and let $\mathbf{F}^\pm, \mathbf{G}^\pm$

be the corresponding diagonal numerical fluxes in (2.9a). We define the isotropic fluxes,

$$\begin{aligned}\widetilde{\mathbf{F}}_{i+\frac{1}{2},j} &= \frac{1}{4}\big(\mathbf{F}^{+}_{i+\frac{1}{2},j+\frac{1}{2}} + 2\mathbf{F}_{i+\frac{1}{2},j} + \mathbf{F}^{-}_{i+\frac{1}{2},j-\frac{1}{2}}\big),\\ \widetilde{\mathbf{G}}_{i,j+\frac{1}{2}} &= \frac{1}{4}\big(\mathbf{G}^{+}_{i+\frac{1}{2},j+\frac{1}{2}} + 2\mathbf{G}_{i,j+\frac{1}{2}} + \mathbf{G}^{-}_{i-\frac{1}{2},j+\frac{1}{2}}\big).\end{aligned} \tag{2.10a}$$

The resulting finite volume scheme reads as

$$\begin{aligned}\frac{d}{dt}\mathbf{U}_{i,j} &= -\frac{1}{\Delta x}\delta_x\widetilde{\mathbf{F}}_{i,j} - \frac{1}{\Delta y}\delta_y\widetilde{\mathbf{G}}_{i,j},\\ &= -\frac{1}{4\Delta x}\left(\delta_/\mathbf{F}^{+}_{i,j} + 2\delta_x\mathbf{F}_{i,j} + \delta_\backslash\mathbf{F}^{-}_{i,j}\right) - \frac{1}{4\Delta y}\left(\delta_/\mathbf{G}^{+}_{i,j} + 2\delta_y\mathbf{G}_{i,j} - \delta_\backslash\mathbf{G}^{-}_{i,j}\right);\end{aligned} \tag{2.10b}$$

here, $\delta_/$ and $\delta_\backslash$ denote the *diagonal* difference operators,

$$\delta_/ a_{I,J} := a_{I+\frac{1}{2},J+\frac{1}{2}} - a_{I-\frac{1}{2},J-\frac{1}{2}}, \quad \delta_\backslash a_{I,J} := a_{I+\frac{1}{2},J-\frac{1}{2}} - a_{I-\frac{1}{2},J+\frac{1}{2}}. \tag{2.11}$$

The GMD structure of the scheme is clear from (2.10b): the scheme averages the fluxes along transverse directions. In contrast to the symmetric scheme (2.5), however, the explicit transverse information in (2.10b) is obtained by "rotating" the fluxes. We term (2.10b) as the *isotropic GMD scheme*.

The stencil of the isotropic scheme consists of nine points. Second-order accuracy can be obtained by the piecewise bilinear reconstruction (1.6). In addition to (1.7), we also need the corner point values,

$$\begin{aligned}\mathbf{U}^{NE}_{i,j} &:= \mathbf{p}_{i,j}(x_{i+\frac{1}{2}}, y_{j+\frac{1}{2}}), \quad \mathbf{U}^{NW}_{i,j} := \mathbf{p}_{i,j}(x_{i-\frac{1}{2}}, y_{j+\frac{1}{2}}),\\ \mathbf{U}^{SE}_{i,j} &:= \mathbf{p}_{i,j}(x_{i+\frac{1}{2}}, y_{j-\frac{1}{2}}), \quad \mathbf{U}^{SW}_{i,j} := \mathbf{p}_{i,j}(x_{i-\frac{1}{2}}, y_{j-\frac{1}{2}}),\end{aligned} \tag{2.12a}$$

and the corresponding diagonal fluxes,

$$\begin{aligned}\mathbf{F}^{+}_{i+\frac{1}{2},j+\frac{1}{2}} &:= \mathbf{F}(\mathbf{U}^{NE}_{i,j}, \mathbf{U}^{SW}_{i+1,j+1}), \quad \mathbf{F}^{-}_{i+\frac{1}{2},j-\frac{1}{2}} := \mathbf{F}(\mathbf{U}^{SE}_{i,j}, \mathbf{U}^{NW}_{i+1,j+1}),\\ \mathbf{G}^{+}_{i+\frac{1}{2},j+\frac{1}{2}} &:= \mathbf{G}(\mathbf{U}^{NE}_{i,j}, \mathbf{U}^{SW}_{i+1,j+1}), \quad \mathbf{G}^{-}_{i-\frac{1}{2},j+\frac{1}{2}} := \mathbf{F}(\mathbf{U}^{NW}_{i,j}, \mathbf{U}^{SE}_{i-1,j+1}),\end{aligned} \tag{2.12b}$$

to define the second order accurate version of the isotropic GMD scheme.

REMARK 2.1. The isotropic GMD scheme (2.10b) is a desirable form of the GMD scheme as we can prove that it is entropy stable provided that the building block numerical fluxes $\mathbf{F}, \mathbf{G}$ in (2.10b) are entropy stable. A precise statement of the stability theorem and details of the proof are presented in [**34**].

3. Numerical Experiments

The semi-discrete first (second) order GMD schemes (2.5), (2.10b) are integrated in time with the standard forward Euler (strong stability preserving Runge-Kutta [**22**]) method. The time step is determined by a standard CFL condition. All simulations reported here, are performed with a CFL number of 0.45. We test the following schemes:

SYM (SYM2)	First (second)-order version of the symmetric GMD scheme (2.5).
ISO (ISO2)	First (second)-order version of the isotropic GMD scheme (2.10b).

3.1. Numerical experiment #1. We begin with a test case for the Euler equations, reported in [**34**]. The two-dimensional radially symmetric version of the standard Sod shock tube [**28**] considers (1.2a) with initial data:

$$\begin{aligned} &\rho(x,y,0) = p(x,y,0) = \begin{cases} 1.0 & \text{if} \quad \sqrt{x^2+y^2} < 0.4, \\ 0.125 & \text{otherwise,} \end{cases} \\ &u(x,y,0) = v(x,y,0) \equiv 0. \end{aligned} \tag{3.1}$$

in the computational domain $[-2,2]\times[-2,2]$. The initial radial discontinuity breaks into an outward propagating shock wave, a contact discontinuity and a rarefaction wave. The waves are radially symmetric and the standard finite volume scheme is known to be deficient, [**28**]. We plot the approximate density at time $t = 0.2$, on a 200×200 mesh in figure 1. The first-order SYM and ISO schemes are diffusive, particularly at the contact discontinuity. The radially symmetric structure is retained and no grid aligned effects or spurious waves are observed. The second-order SYM2 and ISO2 schemes are much more accurate with good resolution at the shock and the contact. The SYM2 scheme leads to small oscillations at the outer shock, indicating that the scheme doesn't contain enough diffusion (similar examples were presented in [**33**]). The second-order ISO2 scheme results in non-oscillatory and resolves the circular waves quite well. The results are comparable to those presented in [**31**] and references therein.

3.2. Numerical experiment #2. As a second example for the Euler equations, we consider a benchmark test described in [**8, 17, 29, 31**] and references therein. The two dimensional initial Riemann data is

$$\begin{aligned} \rho = 0.5313, \quad u = 0, \quad v = 0, \quad p = 0.4, \quad &\text{if} \quad x > 0, y > 0, \\ \rho = 1.0, \quad u = 0, \quad v = 0.7276, \quad p = 1.0, \quad &\text{if} \quad x > 0, y < 0, \\ \rho = 1.0, \quad u = 0.7276, \quad v = 0, \quad p = 1.0, \quad &\text{if} \quad x < 0, y > 0, \\ \rho = 0.8, \quad u = 0, \quad v = 0, \quad p = 1.0, \quad &\text{if} \quad x < 0, y < 0, \end{aligned} \tag{3.2}$$

in the computational domain, $[-1,1]\times[-1,1]$. The exact solution consists of two forward moving shocks, two slip lines and a Mach reflection. Some standard finite volume schemes approximate a regular reflection instead of a Mach reflection, [**17**]. The approximate density at time $t = 0.5$, on a 200×200 mesh, is plotted in figure 2. The results are very similar to the previous numerical experiment. The first-order SYM and ISO schemes resolve the multi-dimensional features with some diffusion. The second-order ISO2 and SYM2 schemes attain considerably better resolution, particularly at the slip lines and at the reflection. The SYM2 scheme has a slight overshoot at the top right corner, indicating the absence of sufficient diffusion. The ISO2 scheme is very stable and accurate. The results are comparable to the ones obtained in [**17, 29, 31**]. The above numerical experiments demonstrate that the GMD schemes presented in this paper are robust. The first order schemes can be diffusive. A possible reason is the use of the Rusanov flux (1.4). Experiments with more accurate fluxes like the Roe flux led to a reduction in the amount of numerical diffusion. We prefer the Rusanov flux as it is very simple to code and is computationally cheap. Furthermore, accuracy is recovered at second-order.

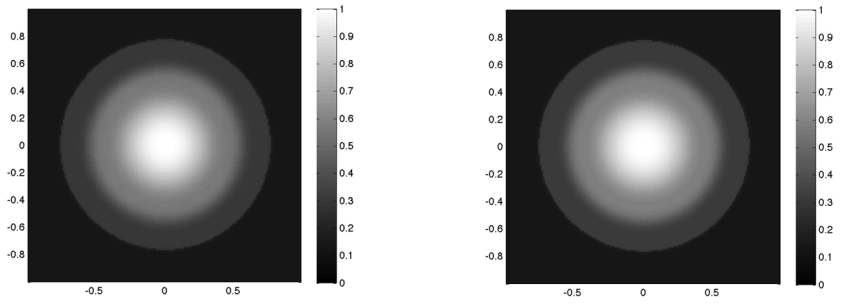

(a) SYM (b) ISO

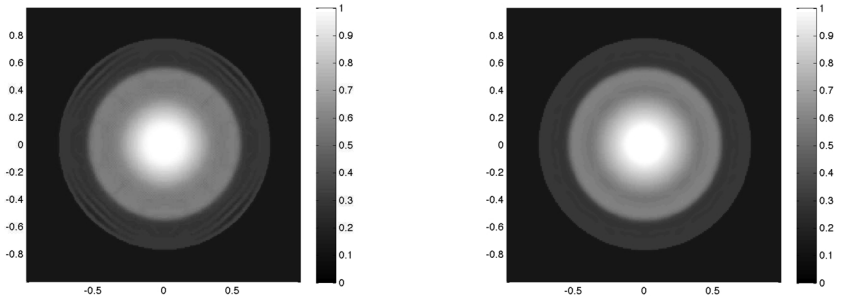

(c) SYM2 (d) ISO2

FIGURE 1. Approximate solutions of density for numerical experiment #3 at $t = 0.2$ on a 200×200 mesh computed with the GMD schemes.

4. Divergence preserving schemes

The divergence of the magnetic field in the MHD equations (1.9) is preserved (1.11a). Despite incorporating explicit transverse information, the GMD schemes (2.5) and (2.10b) may not necessarily preserve a discrete version of the divergence constraint. A possible explanation lies in the special structure of the 8-vectors fluxes $\mathbf{f}$ and $\mathbf{g}$ in (1.9). Note that

$$\mathbf{f}_5 = \mathbf{g}_6 \equiv 0, \quad -\mathbf{f}_6 = \mathbf{g}_5 = u_2 B_1 - u_1 B_2.$$

This *interaction* between the fluxes $\mathbf{f}, \mathbf{g}$ is responsible for the divergence constraint (1.11a). We must incorporate this information in the structure of the numerical potentials.

Let ϕ, ψ be the potentials. Following [**35**], we require that potential components ϕ_5, ϕ_6, ψ_5 and ψ_6 satisfy:

$$(4.1) \quad \left(\phi_5\right)_{i+\frac{1}{2},j+\frac{1}{2}} = \left(\psi_6\right)_{i+\frac{1}{2},j+\frac{1}{2}} \equiv 0, \quad \left(\phi_6\right)_{i+\frac{1}{2},j+\frac{1}{2}} = \left(\psi_5\right)_{i+\frac{1}{2},j+\frac{1}{2}} = \chi_{i+\frac{1}{2},j+\frac{1}{2}}$$

for some consistent scalar potential χ, i.e,

$$\chi(\mathbf{U}, \cdots, \mathbf{U}) = u_1 B_2 - u_2 B_1.$$

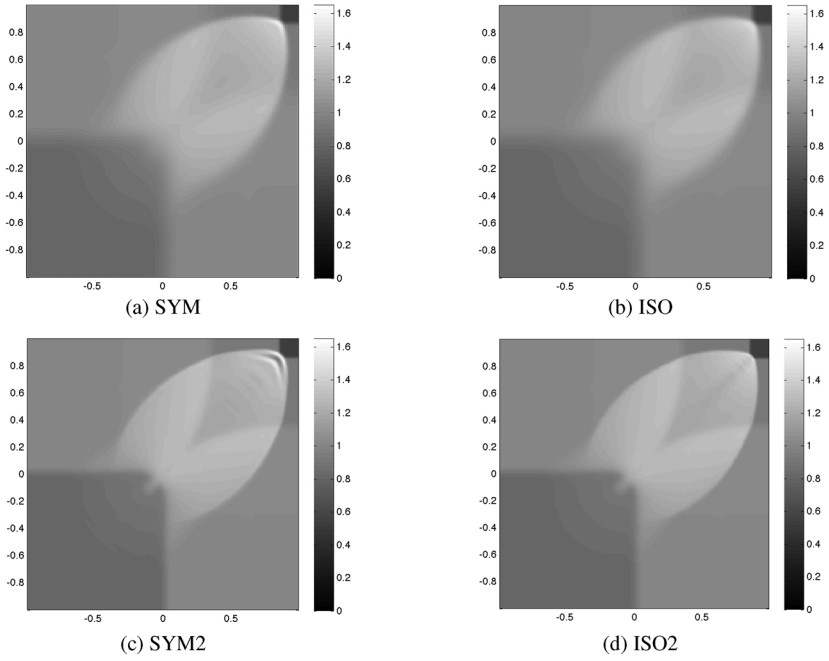

FIGURE 2. Approximate density for numerical experiment #4 at $t = 0.5$ on a 200×200 mesh computed with the GMD schemes.

Introducing

$$\mathbf{V} = \{\rho, u_1, u_2, u_3, B_3, E\}, \quad \Phi = \{\phi_1, \cdots, \phi_4, \phi_7, \phi_8\}, \quad \Psi = \{\psi_1, \cdots, \psi_4, \psi_7, \psi_8\}$$

for any consistent potentials ϕ, ψ. The potential based scheme (2.3) with the choice of potential (4.1) reads as

$$\begin{aligned} \frac{d}{dt}\mathbf{V}_{i,j} &= -\frac{1}{\Delta x}\delta_x\mu_y\Phi_{i,j} - \frac{1}{\Delta y}\delta_y\mu_x\Psi_{i,j}, \\ \frac{d}{dt}\big(B_1\big)_{i,j} &= -\frac{1}{\Delta y}\delta_y\mu_x\chi_{i,j}, \\ \frac{d}{dt}\big(B_2\big)_{i,j} &= \frac{1}{\Delta x}\delta_x\mu_y\chi_{i,j}. \end{aligned} \tag{4.2}$$

The constraint preserving property of the scheme is described in following lemma.

LEMMA 4.1. *Define the discrete divergence operator:*

$$\mathrm{div}^*\big((B_1, B_2)^\top\big)_{i,j} := \frac{1}{\Delta x}\mu_y\delta_x\big(B_1\big)_{i,j} + \frac{1}{\Delta y}\mu_x\delta_y\big(B_2\big)_{i,j}. \tag{4.3}$$

Then, the potential based GMD scheme (4.2) *satisfies the discrete divergence constraint, analogous to* (1.11b)

$$\frac{d}{dt}\mathrm{div}^*\big((B_1, B_2)^\top\big)_{i,j} \equiv 0, \quad \forall i, j.$$

PROOF. The difference operators δ_x, δ_y and the averaging operators μ_x, μ_y commute with each other. Applying the discrete divergence operator div^* to the numerical scheme (4.2),

$$\Delta x \Delta y \frac{d}{dt} \mathrm{div}^* \left((B_1, B_2)^\top\right)_{i,j} = (\mu_x \delta_y \delta_x \mu_y - \mu_y \delta_x \delta_x \mu_x)\chi_{i,j} \equiv 0.$$

□

A similar scheme preserves a discrete version of vorticity for the system wave equation [**34**]. The scalar potential χ can be chosen in the following ways.

4.1. Divergence preserving symmetric GMD scheme. The potentials Φ, Ψ are defined by (2.4). A natural choice [**35**] of the potential χ is the symmetric potential:

$$\chi_{i+\frac{1}{2},j+\frac{1}{2}} = \frac{1}{4}\Big(\big(\mathbf{F}_6\big)_{i+\frac{1}{2},j} + \big(\mathbf{F}_6\big)_{i+\frac{1}{2},j+1} + \big(\mathbf{G}_5\big)_{i,j+\frac{1}{2}} + \big(\mathbf{G}_5\big)_{i+1,j+\frac{1}{2}} \Big) \tag{4.4}$$

with $\mathbf{F}_{5,6}, \mathbf{G}_{5,6}$ being components of any consistent numerical fluxes $\mathbf{F}, \mathbf{G}$. Let

$$\mathbf{H} = \{\mathbf{F}_1, \cdots, \mathbf{F}_4, \mathbf{F}_7, \mathbf{F}_8\}, \quad \mathbf{K} = \{\mathbf{G}_1, \cdots, \mathbf{G}_4, \mathbf{G}_7, \mathbf{G}_8\}$$

for any consistent fluxes $\mathbf{F}, \mathbf{G}$. The divergence preserving symmetric GMD scheme has the explicit form:

$$\begin{aligned}
\frac{d}{dt}\mathbf{V}_{i,j} &= -\frac{1}{2\Delta x}(\mu_y \mathbf{H}_{i+\frac{1}{2},j+\frac{1}{2}} + \mu_y \mathbf{H}_{i+\frac{1}{2},j-\frac{1}{2}} - \mu_y \mathbf{H}_{i-\frac{1}{2},j+\frac{1}{2}} - \mu_y \mathbf{H}_{i-\frac{1}{2},j-\frac{1}{2}}) \\
&\quad - \frac{1}{2\Delta y}(\mu_x \mathbf{K}_{i+\frac{1}{2},j+\frac{1}{2}} + \mu_x \mathbf{K}_{i-\frac{1}{2},j+\frac{1}{2}} - \mu_x \mathbf{K}_{i+\frac{1}{2},j-\frac{1}{2}} - \mu_x \mathbf{K}_{i-\frac{1}{2},j-\frac{1}{2}}), \\
\frac{d}{dt}(B_1)_{i,j} &= -\frac{1}{4\Delta y}\Big(\mu_x \big(\mathbf{F}_6\big)_{i,j+1} - \mu_x \big(\mathbf{F}_6\big)_{i,j-1}\Big) - \frac{1}{4\Delta y}\Big(\delta_y(\mu_x \big(\mathbf{G}_5\big)_{i+\frac{1}{2},j+\frac{1}{2}} + \mu_x \big(\mathbf{G}_5\big)_{i-\frac{1}{2},j+\frac{1}{2}})\Big), \\
\frac{d}{dt}(B_2)_{i,j} &= \frac{1}{4\Delta x}\Big(\mu_y \big(\mathbf{G}_5\big)_{i+1,j} - \mu_y \big(G_5\big)_{i-1,j}) + \frac{1}{4\Delta x}(\delta_x(\mu_y \big(\mathbf{F}_6\big)_{i+\frac{1}{2},j+\frac{1}{2}} + \mu_y \big(\mathbf{F}_6\big)_{i+\frac{1}{2},j-\frac{1}{2}})\Big).
\end{aligned} \tag{4.5}$$

4.2. Divergence preserving isotropic GMD scheme. Following [**33**], we define a *diagonal* form of the potential χ:

$$\chi_{i+\frac{1}{2},j+\frac{1}{2}} = \frac{1}{4}\Big(\big(\mathbf{F}_6^+\big)_{i+\frac{1}{2},j+\frac{1}{2}} + \big(\mathbf{G}_5^+\big)_{i+\frac{1}{2},j+\frac{1}{2}} + \big(\mathbf{F}_6^-\big)_{i+\frac{1}{2},j+\frac{1}{2}} + \big(\mathbf{G}_5^-\big)_{i+\frac{1}{2},j+\frac{1}{2}} \Big) \tag{4.6}$$

for diagonal fluxes $\mathbf{F}^\pm, \mathbf{G}^\pm$ defined in (2.9b). Denote

$$\mathbf{H}^\pm = \{\mathbf{F}_1^\pm, \cdots, \mathbf{F}_4^\pm, \mathbf{F}_7^\pm, \mathbf{F}_8^\pm\}, \quad \mathbf{K}^\pm = \{\mathbf{G}_1^\pm, \cdots, \mathbf{G}_4^\pm, \mathbf{G}_7^\pm, \mathbf{G}_8^\pm\}$$

The divergence preserving modification of the isotropic GMD scheme (2.10b) based on the potential (4.6) is

$$\begin{aligned}
\frac{d}{dt}\mathbf{V}_{i,j} &= -\frac{1}{4\Delta x}\left(\delta_/ \mathbf{H}^+_{i,j} + 2\delta_x \mathbf{H}_{i,j} + \delta_\backslash \mathbf{H}^-_{i,j}\right) - \frac{1}{4\Delta y}\left(\delta_/ \mathbf{K}^+_{i,j} + 2\delta_y \mathbf{K}_{i,j} - \delta_\backslash \mathbf{K}^-_{i,j}\right), \\
\frac{d}{dt}(B_1)_{i,j} &= -\frac{1}{4\Delta y}\left(\mu_x \delta_y \Big(\big(\mathbf{F}_6^+\big)_{i,j} + \big(\mathbf{F}_6^-\big)_{i,j} + \big(\mathbf{G}_5^+\big)_{i,j} + \big(\mathbf{G}_5^-\big)_{i,j} \Big)\right), \\
\frac{d}{dt}(B_2)_{i,j} &= \frac{1}{4\Delta x}\left(\mu_y \delta_x \Big(\big(\mathbf{F}_6^+\big)_{i,j} + \big(\mathbf{F}_6^-\big)_{i,j} + \big(\mathbf{G}_5^+\big)_{i,j} + \big(\mathbf{G}_5^-\big)_{i,j} \Big)\right).
\end{aligned} \tag{4.7}$$

4.3. Numerical Experiments. In addition to the SYM (SYM2) and ISO (ISO2) schemes of the last section, we also test the following two divergence preserving GMD schemes:

SCP (SCP2) —
First (second)-order version of the divergence preserving symmetric GMD scheme (4.5);

ICP (ICP2) —
First (second)-order version of the divergence preserving isotropic GMD scheme (4.7).

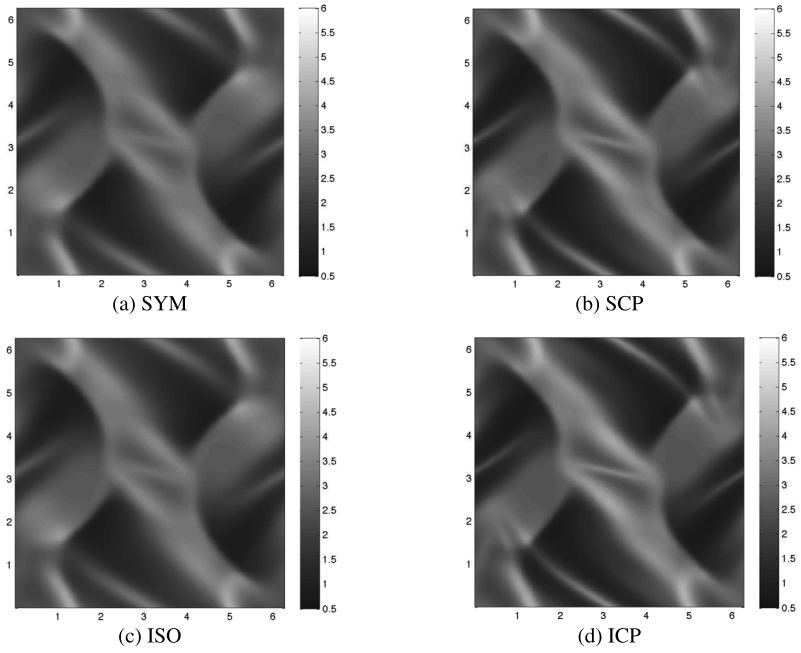

FIGURE 3. The pressure p for the Orszag-Tang vortex computed at $t = \pi$ on a 200×200 mesh with first-order GMD schemes.

4.4. Orszag-Tang vortex. The Orszag-Tang vortex is a widely reported benchmark for multi-dimensional MHD equations [**48**]. The initial data is

$$(\rho, u_1, u_2, u_3, B_1, B_2, B_3, p) = \left(\gamma^2, -\sin(y), \sin(x), 0, -\sin(y), \sin(2x), 0, \gamma\right),$$

in the computational domain, $(x, y, t) \in [0, 2\pi]^2 \times [0, \pi]$ with periodic boundary conditions.

Although the exact solution is not known, some qualitative features have been reported [**48**]. The solution consists of shocks along the diagonals and interesting smooth features including a vortex near the center of the domain. The approximate pressures, computed on a 200×200 mesh, are shown in figures 3 and 4.

Figure 3 shows the approximate pressure computed with the first-order GMD schemes. The solution is smeared at this resolution, but the qualitative features are captured quite well. The shocks and the central vortex are approximated, without any spurious waves or oscillations. The divergence preserving SCP and ICP schemes are clearly more accurate than the SYM and ISO schemes. The

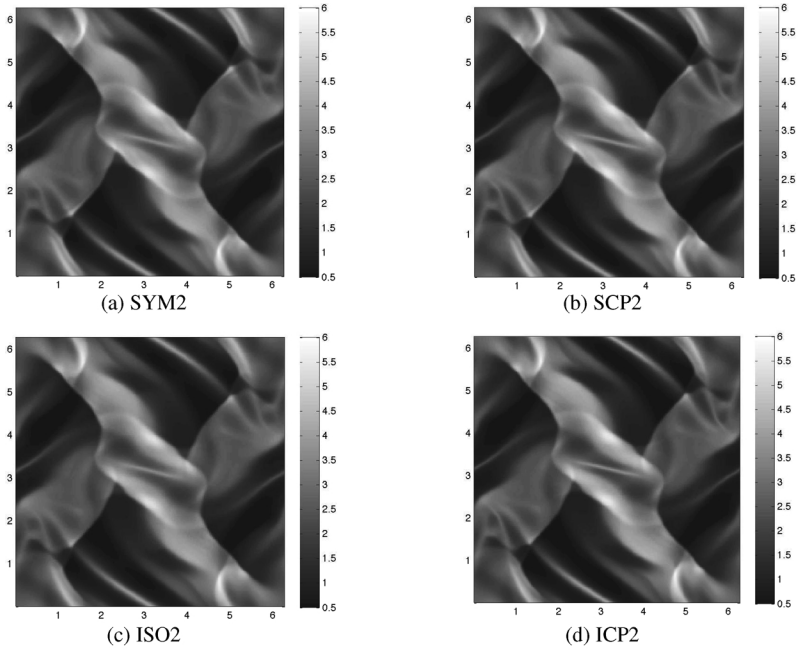

FIGURE 4. The pressure p for the Orszag-Tang vortex computed at $t = \pi$ on a 200×200 mesh with second-order GMD schemes.

results for the second-order schemes are plotted in figure 4. There is a considerable improvement in the resolution with second-order schemes. The gain in accuracy is evident, both at the shocks and at the central vortex. The divergence preserving SCP2 and ICP2 are slightly more accurate than the SYM2 and ISO2 schemes.

The initial data is divergence free and the divergence constraint (1.11a) implies that it remains zero during the evolution. We show the errors in the discrete divergence operator div^* (4.3) in Table 1. The standard GMD schemes lead to

M	SYM	ISO	SCP	ICP	SYM2	ISO2	SCP2	ICP2
50	0.53	0.42	4.7e-12	4.4e-12	1.49	1.32	5.8e-13	3.4e-13
100	0.89	0.70	2.1e-12	1.7e-12	3.39	3.07	5.1e-13	3.8e-13
200	1.23	1.11	1.0e-12	6.9e-13	5.57	5.12	5.7e-13	3.0e-13
400	1.61	1.52	1.3e-12	6.0e-13	8.08	11.3	6.0e-13	3.1e-13

TABLE 1. Discrete divergence div^* (4.3) in L^1 for the Orszag-Tang vortex with all the GMD schemes on a $M \times M$ mesh at time $t = \pi$.

$\mathcal{O}(1)$ divergence errors, with large amounts of discrete divergence being generated near the shocks. The divergence error is even larger for the second-order SYM2 and ISO2 schemes. This behavior is to be expected as the second-order schemes resolve the shocks more sharply. The SCP, SCP2, ICP and ICP2 schemes preserve

the discrete divergence to machine precision. We would like to point out that preserving div^* to machine precision would imply that other discrete versions of the divergence operator like the standard central divergence will be of the order of machine precision for smooth solutions. Since, the above example contains strong shocks, large values for the standard central divergence may be observed even if div^* is preserved to machine precision.

Numerical stability (particularly on fine meshes) for the MHD equations is delicate [**19**]. Standard schemes (even those with divergence cleaning) may crash due to instabilities and negative pressures on fine resolutions [**19**]. In spite of the large divergence errors, the SYM (SYM2) and ISO (ISO2) schemes are stable. The genuinely multi-dimensional structure of the schemes imparts additional numerical stability.

4.5. Cloud-Shock Interaction. Another benchmark test case for the MHD equations involves the interaction of a high density cloud with a shock. The initial data for this cloud-shock interaction problem [**42**] consists of a shock located at $x = 0.05$ with

$$(\rho, u_1, u_2, u_3, B_1, B_2, B_3, p) = \begin{cases} (3.86859, 11.2536, 0, 0, 0, 2.1826182, -2.1826182, 167.345), & \text{if } x < 0.05 \\ (1.0, 0, 0, 0, 0, 0.56418958, 0.56418958, 1.0), & \text{if } x < 0.05. \end{cases} \tag{4.8}$$

and a circular cloud of density $\rho = 10$ with radius 0.15, centered at $(x, y) = (0.25, 0.5)$ in the computational domain $[0, 1] \times [0, 1]$. The test is configured in such a way that a right moving shock violently interacts with a high density cloud. The solution has a extremely complex structure, consisting of bow shock at the left, trailing shocks at the right and a complicated smooth region with turbulent like features in the center. We plot the approximate density, on a 200×200 mesh , at time $t = 0.06$ in figures 5 and 6.

The first-order results in figure 5 show that although diffusive, the first-order GMD schemes are stable and resolve the shock structure in the correct qualitative manner. The divergence preserving SCP and ICP schemes are more accurate than the SYM and ISO schemes. The second-order results are plotted in figure 6 and show a *dramatic* increase in resolution. Both the bow shock and the trailing shock are captured accurately. The smooth region with turbulent features is also resolved quite well. In fact, a clear difference between the first- and second-order schemes lies in the fact that the second-order schemes resolve some of the turbulent features on very coarse meshes. The divergence errors for discrete divergence div^* are shown in Table 2 and demonstrate quite large divergence errors for the SYM (SYM2) and ISO (ISO2) schemes. The divergence errors increase with reduction in mesh size, indicating production of divergence at the shocks. The SCP (SCP2) and ICP (ICP2) schemes preserve discrete divergence to machine precision.

5. Conclusion

The structure of solutions of conservation laws in several space dimensions is very rich and consists of complex multi-dimensional waves. Standard finite volume methods are based on edge centered fluxes and do not incorporate any explicit transverse information. Consequently, they are deficient in resolving genuinely

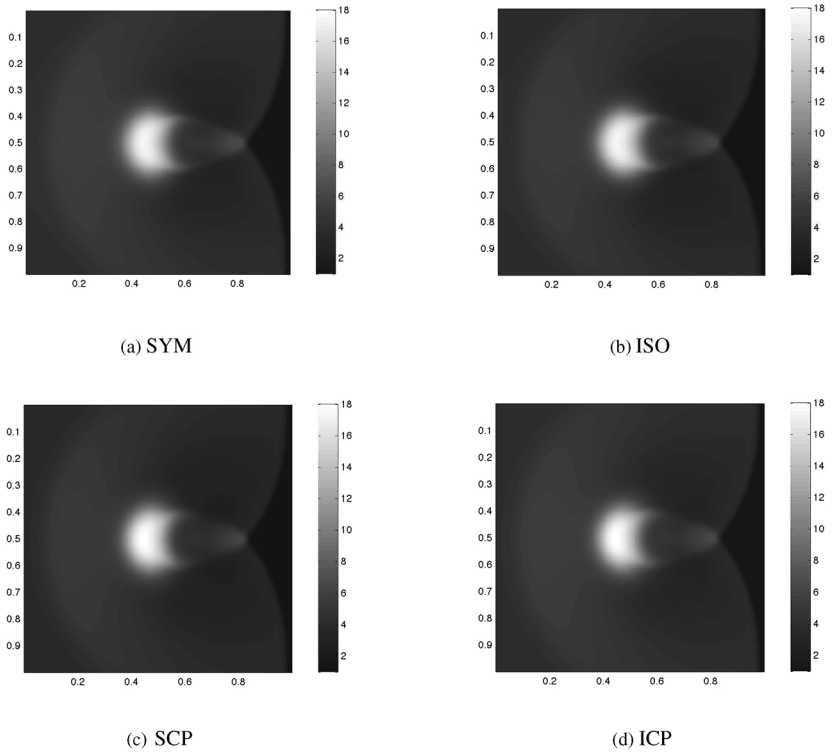

(a) SYM (b) ISO

(c) SCP (d) ICP

FIGURE 5. The density ρ for the cloud-shock interaction computed at $t = 0.06$ on a 200×200 mesh with first-order schemes.

M	SYM	ISO	SCP	ICP	SYM2	ISO2	SCP2	ICP2
50	4.56	2.59	2.8e-12	2.1e-12	5.79	5.38	3.4e-13	2.27e-13
100	4.47	3.3	1.2e-12	8.7e-13	12.58	11.75	2.1e-13	1.14e-13
200	5.19	4.05	5.0e-13	3.7e-13	27.1	26.48	1.4e-13	1.34e-13
400	7.5	6.4	2.3e-13	1.5e-13	38.0	41.3	1.8e-13	2.2e-13

TABLE 2. Discrete divergence div^* (4.3) in L^1 for cloud shock interaction with all the eight schemes on a $M \times M$ mesh at time $t = 0.06$.

multi-dimensional waves. These deficiencies are particularly evident for conservation laws with intrinsic constraints like vorticity and divergence. Finite volume schemes may not preserve discrete versions of the constraint and may lead to spurious numerical waves and oscillations.

We summarize the results of a recent series of papers [**33, 34, 35**] where a new framework for genuinely multi-dimensional (GMD) schemes was presented. These schemes are based on vertex centered numerical potentials. Standard edge centered fluxes are used to define the potentials. A particular version of the GMD schemes, he isotropic GMD scheme (2.10b) is entropy stable if its building block numerical fluxes are entropy stable.

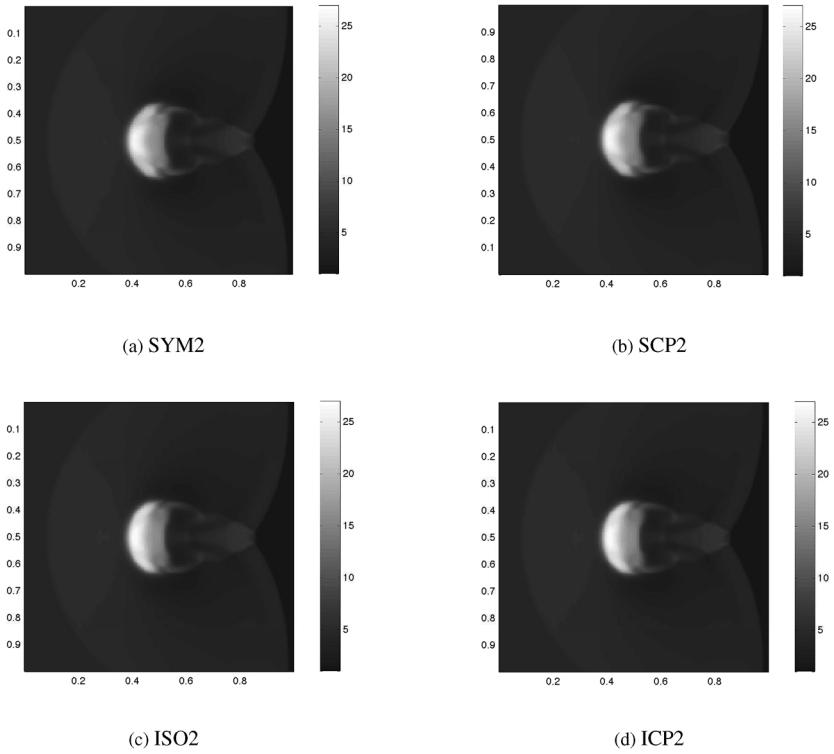

(a) SYM2 (b) SCP2

(c) ISO2 (d) ICP2

FIGURE 6. The density ρ for the cloud-shock interaction computed at $t = 0.06$ on a 200×200 mesh with second-order schemes

A suitable choice of potentials leads to a GMD scheme that preserves discrete version of the divergence constraint for the ideal MHD equations (1.9). Higher order of spatial accuracy is obtained by employing the non-oscillatory reconstruction procedure of [**25**]. A choice of the Rusanov flux as the building block for the GMD schemes leads to genuinely multi-dimensional and constraint preserving versions of the popular central schemes of Kurganov and Tadmor [**25**].

Numerical experiments for the Euler and the MHD equations are presented. They show that the GMD schemes are robust and resolve the multi-dimensional waves with high accuracy. Preserving the divergence constraint leads to higher resolution, particularly at first-order. The computational cost of the schemes are very low and they are very simple to implement in a code. Hence, the GMD framework constitutes an unified and highly effective strategy for approximating multi-dimensional conservation laws. Future papers consider higher than second-order versions of the GMD schemes on unstructured grids.

References

[1] R. Artebrant and M.Torrilhon. Increasing the accuracy of local divergence preserving schemes for MHD. *J. Comp. Phys.*, 227 (6), 3405-3427, 2008.

[2] R. Abgrall and P. L. Roe. High-order fluctuation schemes on triangular meshes. *SIAM J. sci. comput.,* 198, 3 -36, 2003.

[3] J. Balbás and E. Tadmor. Non-oscillatory central schemes for one and two-dimensional magnetohydrodynamics II: High-order semi-discrete schemes. *SIAM. J. Sci. Comput.,* 28 (2), 533-560, 2006.
[4] J. Balbás , E. Tadmor and C. C. Wu. Non-oscillatory central schemes for one and two-dimensional magnetohydrodynamics I. *J. Comp. Phys.,* 201 (1), 261-285, 2004.
[5] D. S. Balsara and D. Spicer. A staggered mesh algorithm using high order Godunov fluxes to ensure solenoidal magnetic fields in magnetohydrodynamic simulations. *J. Comp. Phys.*, 149(2):270-292, 1999.
[6] J. B. Bell, P. Colella and H. M. Glaz. A second-order projection method for the incompressible Navier-Stokes equations. *J. Comp. Phys.*, 85, 257-283, 1989.
[7] J. U. Brackbill and D. C. Barnes. The effect of nonzero Div$B$ on the numerical solution of the magnetohydrodynamic equations. *J. Comp. Phys.*, 35:426-430, 1980.
[8] M. Brio, A. R. Zakharian, and G. M. Webb. Two-dimensional Riemann solver for Euler equations of gas dynamics. *J. Comp. Phys.,* 167 (1):177-195, 2001.
[9] M. Brio and C. C. Wu. An upwind differencing scheme for the equations of ideal MHD. *J. Comp. Phys,* 75 (2), 1988, 400 - 422.
[10] A. J. Chorin. Numerical solutions of the Navier-Stokes equations. *Math. Comp.*, 22, 745-762, 1968.
[11] P. Colella. Multi-dimensional upwind methods for hyperbolic conservation laws. *J. Comp. Phys.,* 87, 171-200, 1990.
[12] C. Dafermos. *Hyperbolic conservation laws in continuum physics.* Springer, Berlin, 2000.
[13] W. Dai and P. R. Woodward. A simple finite difference scheme for multi-dimensional magnetohydrodynamic equations. *J. Comp. Phys.*, 142(2):331-369, 1998.
[14] H. Deconnik, P. L. Roe and R. Struijs. A multi-dimensional generalization of Roe's flux difference splitter for Euler equations. *Comput. Fluids*, 22, 215, 1993.
[15] A. Dedner, F. Kemm, D. Kröner, C. D. Munz, T. Schnitzer and M. Wesenberg. Hyperbolic divergence cleaning for the MHD equations. *J. Comp. Phys.,* 175, 645-673, 2002.
[16] C. Evans and J. F. Hawley. Simulation of magnetohydrodynamic flow: a constrained transport method. *Astrophys. J.*, 332:659, 1998.
[17] M. Fey. Multi-dimensional upwingding.(I) The method of transport for solving the Euler equations. *J. Comp. Phys.,* 143(1): 159-180, 1998.
[18] M. Fey. Multi-dimensional upwingding.(II) Decomposition of Euler equations into advection equations. *J. Comp. Phys.,* 143(1): 181-199, 1998.
[19] F. Fuchs, S. Mishra and N.H. Risebro. Splitting based finite volume schemes for ideal MHD equations. *J. Comp. phys,*, 228 (3): 641-660, 2009.
[20] F. Fuchs, A. D. McMurry, S. Mishra, N. H. Risebro and K. Waagan. Approximate Riemann solver based high order finite volume schemes for the Godunov-Powell form of the ideal MHD equations in multi dimensions. *Preprint,* 2009.
[21] S. K. Godunov. The symmetric form of magnetohydrodynamics equation. *Num. Meth. Mech. Cont. Media*, 1:26-34, 1972.
[22] S. Gottlieb, C. W. Shu and E. Tadmor. High order time discretizations with strong stability property. *SIAM. Review,* 43, 2001, 89 - 112.
[23] A. Harten, B. Engquist, S. Osher and S. R. Chakravarty. Uniformly high order accurate essentially non-oscillatory schemes. *J. Comput. Phys.*, 1987, 231-303.
[24] R. Jeltsch and M. Torrilhon. On curl preserving finite volume discretizations of the shallow water equations. *BIT*, 46, 2006, suppl.
[25] A. Kurganov and E. Tadmor. New high resolution central schemes for non-linear conservation laws and convection-diffusion equations. *J. Comput. Phys*, 160(1), 241-282, 2000.
[26] A. Kurganov, S. Noelle and G. Petrova. Semi-discrete central upwind schemes for hyperbolic conservation laws and Hamilton-Jacobi equations. *SIAM J. Sci. comput.,* 23(3), 707 - 740, 2001.
[27] B. van Leer Towards the Ultimate Conservative Difference Scheme, V. A Second Order Sequel to Godunov's Method. *J. Com. Phys.,* 32, 101136, 1979.
[28] R. J. LeVeque. Finite volume methods for hyperbolic problems. *Cambridge university press,* Cambridge, 2002.
[29] R. J. LeVeque. Wave propagation algorithms for multi-dimensional hyperbolic systems, *J. Comp. Phys.,* 131, 327-353, 1997.

[30] M. Lukacova-Medvidova, K. W. Morton and G. Warnecke. Evolution Galerkin methods for Hyperbolic systems in two space dimensions. *Math. Comp.,* 69 (232), 1355 - 1384, 2000.
[31] M. Lukacova-Medvidova, J. Saibertova and G. Warnecke. Finite volume evolution Galerkin methods for Non-linear hyperbolic systems. *J. Comp. Phys.,* 183, 533 - 562, 2003.
[32] M. Lukacova-Medvidova and J. Saibertova. Finite volume schemes for multi-dimensional hyperbolic systems based on use of bi-characteristics. *Appl. Math.,* 51 (3), 205 - 228, 2006.
[33] S. Mishra and E. Tadmor, Constraint preserving schemes using potential-based fluxes. I. Multi-dimensional transport equations. *Preprint,* 2009.
[34] S. Mishra and E. Tadmor, Constraint preserving schemes using potential-based fluxes. II. Genuinely multi-dimensional central schemes for systems of conservation laws. *Preprint,* 2009.
[35] S. Mishra and E. Tadmor, Constraint preserving schemes using potential-based fluxes. III. Genuinely multi-dimensional central schemes for MHD equations. *Preprint,* 2009.
[36] K. W. Morton and P. L. Roe. Vorticity preserving Lax-Wendroff type schemes for the system wave equation. *SIAM. J. Sci. Comput.,* 23 (1), 2001, 170-192.
[37] H. Nishikawa and P. L. Roe. Towards high-order fluctuation-splitting schemes for Navier-Stokes equations. *AIAA paper*, 2005-5244, 2005.
[38] S. Noelle. The MOT-ICE: A new high-resolution wave propagation algorithm for multi-dimensional systems of conservation laws based on Fey's method of transport. *J. Comp. Phys.,* 164, 283 - 334, 2000.
[39] K. G. Powell. An approximate Riemann solver for magneto-hydro dynamics (that works in more than one space dimension). Technical report, 94 -24, ICASE, Langley, VA, 1994.
[40] K. G. Powell, P. L. Roe. T. J. Linde, T . I. Gombosi and D . L. De zeeuw, A solution adaptive upwind scheme for ideal MHD. J. Comp. Phys, 154(2), 284 - 309, 1999
[41] P. L. Roe and D. S. Balsara. Notes on the eigensystem of magnetohydrodynamics. *SIAM. J. Appl. Math.*, 56 (1), 1996, 57 - 67.
[42] J. Rossmanith. A wave propagation method with constrained transport for shallow water and ideal magnetohydrodynamics. Ph.D thesis, University of Washington, Seattle, 2002.
[43] D. S. Ryu, F. Miniati, T. W. Jones and A. Frank. A divergence free upwind code for multidimensional magnetohydrodynamic flows. *Astrophys. J.*, 509(1):244-255, 1998.
[44] C. W. Shu and S. Osher. Efficient implementation of essentially non-oscillatory schemes - II, *J. Comput. Phys.*, 83, 1989, 32 - 78.
[45] E. Tadmor. Approximate solutions of nonlinear conservation laws. *Advanced Numerical approximations of Nonlinear Hyperbolic equations, A. Quarteroni ed.*, Lecture notes in Mathematics, Springer Verlag (1998), 1-149.
[46] M. Torrilhon. Locally divergence preserving upwind finite volume schemes for magneto-hydro dynamics. *SIAM. J. Sci. Comp.*, 26 (4), 1166-1191, 2005.
[47] M. Torrilhon and M. Fey. Constraint-preserving upwind methods for multidimensional advection equations. *SIAM. J. Num. Anal.*, 42(4):1694-1728, 2004.
[48] G. Toth. The Div$B$ = 0 constraint in shock capturing magnetohydrodynamics codes. *J. Comp. Phys.*,161:605-652, 2000.

(Siddhartha Mishra)
Seminar for Applied Mathematics
D-MATH, ETH
Rämistrasse,
8092, Zürich, Switzerland
E-mail address: smishra@sam.math.ethz.ch

(Eitan Tadmor)
Department of Mathematics
Center of Scientific Computation and Mathematical Modeling (CSCAMM)
Institute for Physical sciences and Technology (IPST)
University of Maryland
MD 20741-4015, USA
E-mail address: tadmor@cscamm.umd.edu